HHS Public Access

Author manuscript

Circ Cardiovasc Imaging. Author manuscript; available in PMC 2017 April 03.

Published in final edited form as:

Circ Cardiovasc Imaging. 2016 November ; 9(11): . doi:10.1161/CIRCIMAGING.116.004731.

Magnetic Resonance Imaging of Cardiac Strain Pattern Following Transplantation of Human Tissue Engineered Heart Muscles

Xulei Qin, PhD[*], **Johannes Riegler, PhD**[*], **Malte Tiburcy, MD**, **Xin Zhao, MD, PhD**, **Tony Chour, BS**, **Babacar Ndoye, BS**, **Michael Nguyen, BS**, **Jackson Adams, BS**, **Mohamed Ameen, BS**, **Thomas S. Denney Jr., PhD**, **Phillip C. Yang, MD**, **Patricia Nguyen, MD**, **Wolfram H. Zimmermann, MD**, and **Joseph C. Wu, MD, PhD**

Stanford Cardiovascular Institute and Department of Medicine, Division of Cardiology, Stanford, CA (X.Q., J.R., X.Z., T.C., B.D., M.T.N., J.A., M.A., P.C.Y., P.N., J.C.W.); Auburn University MRI Research Center, Department of Electrical and Computer Engineering, Auburn University, Auburn, AL (T.S.D.Jr.); Institute of Pharmacology, Heart Research Center, University Medical Center, Georg-August-University and German Center for Cardiovascular Research, Göttingen, Germany (M.T., W.H.Z.)

Abstract

Background—The use of tissue engineering approaches in combination with exogenously produced cardiomyocytes offers the potential to restore contractile function after myocardial injury. However, current techniques assessing changes in global cardiac performance following such treatments are plagued by relatively low detection ability. As the treatment is locally performed, this detection could be improved by myocardial strain imaging that measures regional contractility.

Methods and Results—Tissue engineered heart muscles (EHMs) were generated by casting human embryonic stem cell-derived cardiomyocytes with collagen in preformed molds. EHMs were transplanted (n=12) to cover infarct and border zones of recipient rat hearts one month after ischemia reperfusion injury. A control group (n=10) received only sham placement of sutures without EHMs. To assess the efficacy of EHMs, MRI and ultrasound-based strain imaging were performed prior to and four weeks after transplantation. In addition to strain imaging, global cardiac performance was estimated from cardiac MRI. Although no significant differences were found with global changes in left ventricular ejection fraction (EF) (Control −9.6±1.3% vs. EHM −6.2±1.9%, P=0.17), regional myocardial strain from tagged MRI was able to detect preserved systolic function in EHM-treated animals compared to control (Control 4.4±1.0% vs. EHM 1.0±0.6%, P=0.04). However, ultrasound-based strain failed to detect any significant change (Control 2.1±3.0% vs. EHM 6.3±2.9%, P=0.46).

Correspondence: Dr. Joseph C. Wu, 265 Campus Drive, Room G1120B, Stanford, CA 94305-5454. joewu@stanford.edu.

[*]X.Q. and J.R. contributed equally to this study.

Disclosures

None

Conclusions—This study highlights the feasibility of using cardiac strain from tagged MRI to assess functional changes in rat models due to localized regenerative therapies, which may not be detected by conventional measures of global systolic performance.

Keywords

myocardial infarction; tissue engineering; engineered heart muscle; MRI; strain imaging

INTRODUCTION

Engineered heart muscles (EHMs) are macroscopic tissue constructs generated from either embryonic stem cell-derived cardiomyocytes (ESC-CMs) or induced pluripotent stem-cell derived cardiomyocytes (iPSC-CMs) and collagen. Transplantation of EHMs leads to engraftment and long-term survival of up to 25% of transplanted cardiomyocytes.[1, 2] Furthermore, pre-clinical studies have indicated the therapeutic potential of this approach to preserve contractile function after myocardial infarction (MI).[3–5] To assess the therapeutic potential and optimize tissue engineering and transplantation procedures, an evaluation method that can assess localized contractile performance is required. Noninvasive imaging techniques such as cardiac ultrasound and magnetic resonance imaging (MRI) are indispensable for this task.[6, 7] Cardiac ultrasound is a fast, inexpensive, and convenient technique to evaluate systolic function, which has led to its widespread application in both pre-clinical and clinical trials for cardiac stem cell therapies.[8, 9] Cardiac MRI, which offers high resolution and superior soft tissue contrast, has also been utilized to evaluate the therapeutic efficacy of stem cell therapies.[4, 10, 11] MRI has become the gold standard for the assessment of cardiac function due to its advantages.[12, 13]

However, most studies to date have relied on global estimates of systolic function such as left ventricular ejection fraction (EF) to assess therapeutic interventions. Although these global measurements are convenient standards for evaluating cardiac function, they have limited ability to detect small localized changes in myocardial function.[14, 15] Accurate assessment of localized changes in contractile function is particularly important for therapies that are applied to a small region of the heart, such as intramyocardial injections of CMs or transplantation of EHMs in the border zone of the scar region.[16]

The development of cardiac strain imaging techniques has enabled the assessment of regional myocardial deformations in beating rodent and human hearts.[17–19] Two frequently used methods for myocardial strain imaging are tagged MRI and ultrasound-based speckle tracking. Tagged MRI is a technique that applies a grid pattern on myocardial tissue at the beginning of the cardiac cycle by nulling the MRI signal of tag lines (grid lines), followed by imaging the displacement of tag lines throughout the cardiac cycle. Tracking of tag line displacements due to cardiac contractions enables the measurement of myocardial deformations and strains in three dimensions (3D). Alternative methods that do not rely on intensive post processing for tag line tracking have been developed more recently.[14, 20, 21] Cardiac ultrasound strain imaging techniques, such as tissue Doppler and speckle tracking from B-mode images, have been developed to quantify segmental motion and deformations of the myocardium by post-processing of velocity data or grayscale images. Ultrasound-

based strain imaging has been widely used to investigate hypertrophic cardiomyopathies and coronary artery diseases.[22–24] Although strain imaging has been applied for the diagnosis of regional myocardial dysfunction in clinics, its ability to detect regional function changes after localized therapeutic intervention still needs to be validated.

To this end, we set out to evaluate the feasibility of MRI and ultrasound-based strain imaging techniques to detect changes in regional myocardial function following EHM transplantation. We used EHM transplantation or sham suture placement (control) at four weeks after rat myocardial ischemia reperfusion injury to model chronic heart failure. We performed cardiac MRI and ultrasound one day before and four weeks after EHM or sham transplantation to assess the changes in systolic function, using conventional global-based and regional strain-based measurements and subsequently comparing their detection abilities.

METHODS

EHM Generation

Human H7 embryonic stem cells (ESCs; WiCell, Madison, WI) were expanded and differentiated into cardiomyocytes using a small molecule protocol.[25] EHMs were generated by casting human ESC-CMs with collagen in preformed molds following a previously published protocol.[26] After condensing for five days, EHMs were transferred to mechanical stretchers for functional maturation for 12–14 days.

Myocardial Infarction and EHM Transplantation

All animal procedures were performed in accordance with Stanford's Administrative Panel on Laboratory Animal Care (APLAC) protocol. MI was induced in 8 to 10-week old male nude athymic rats (Charles River, Wilmington, MA). The left anterior descending (LAD) coronary artery was occluded for 60 min followed by reperfusion. One month after MI surgery, rats underwent baseline MRI. Following pilot experiments with an effect size of 5% and a standard deviation of 4% of myocardial strain changes, a power calculation indicated each group size of 10 should be sufficient to detect the treatment effect with a power of 0.8 and Type I error rate of 0.05. Based on previous experiments, we expected to use 80% of animals operated on for randomization (n=22). These rats with sufficient functional impairment (EF <65%, baseline EF before surgery was 73±1%) were randomly assigned to treatment (n=12) or control (n=10) groups in blocks of 2–3. Moreover, some rats were imaged before any surgery as a baseline group (n=6). One day after baseline assessment, a second thoracotomy was performed, and EHMs were placed over the scar region and sutured onto the left ventricular free wall using 8–12 stitches (7-0 Prolene) (Figure 1A). Animals in the control group underwent the same procedure without EHM placement, receiving only sham sutures on the left ventricle (LV). Surgeries were performed under isoflurane anesthesia (1.5–2%) using aseptic techniques.

Cardiac MRI

Cardiac MRI was performed one day before (D-1) and 28 days after (D28) EHM transplantation or sham surgery using a 7T MR901 Discovery horizontal bore scanner

(Agilent Technologies, Santa Clara, CA) with a shielded gradient system (600 mT/m). Rats were anesthetized with 1–2% (v/v) isoflurane in oxygen, kept at 37±0.4 °C via an air heating system, and placed in prone position on an animal cradle. During imaging, rats were kept in the center of a decoupled 72 mm transmit/receive volume coil (Agilent) and data were acquired from a 4-channel phased array receive-only surface coil (Rapid MR International, Columbus, OH) placed around the chest. Electrocardiogram, respiration, and temperature were synchronously recorded to monitor animal health and trigger the MRI acquisitions. Cardiac function, scar size, and localized contractility were assessed by cine MRI, late gadolinium-enhanced (LGE), and tagged MRI, respectively. Total MRI scan time was approximately one hour.

Cine MRI—Following scout acquisitions to define long- and short-axis views, cine imaging was performed to evaluate global systolic function. An ECG and respiration-gated spoiled gradient echo sequence was used to acquire 20 frames covering the cardiac cycle: echo time (TE) 1.5 ms, repetition time (TR) 6–8 ms, flip angle 15°, FOV 50×50 mm^2, in plain resolution 0.2×0.2 mm^2, slice thickness 1 mm, no slice gap. Two and four chamber long-axis views as well as 14–15 short-axis slices were acquired to cover the heart from apex to base.

Tagged MRI—Tagged imaging was performed after cine image acquisitions. A double-gated spatial modulation of magnetization (SPAMM) tagging preparation with a tag spacing of 7 voxels was used to generate a grid-like tagging pattern, followed by fast gradient echo readouts. Tagged MRI images were acquired using slice localizations defined for cine imaging but with different acquisition parameters: TE 1.5 ms, TR 6–8 ms, flip angle 10°, FOV 40×40 mm^2, in plain resolution 0.16×0.16 mm^2, slice thickness 1 mm, spacing 1.6 mm, NSA 3, 20 frames for each R-R interval. The tagged images from short-axis (sparsely imaged every third slice), two chamber, and four chamber views were acquired to cover the 3D heart geometry.

LGE MRI—Finally, to identify the scar location and quantify its size, LGE images were acquired 8 min after intravenous infusion of gadolinium (0.8 mmol/kg; Magnevist Bayer, Germany). An inversion recovery gradient echo sequence with inversion time optimized to null the healthy myocardium signal was used with the following imaging parameters: TE 1.4 ms, TR one breathing interval, TI 280–370 ms, flip angle 90°, slice thickness 1 mm, no slice separation, FOV 40×40 mm^2, matrix size 192×192, NSA 2, and views per segment 2.

Image analysis and strain calculation—Images were blinded for analysis. Both endocardial and epicardial borders were automatically segmented on cine images following manual correction by an experienced user using Segment (http://segment.heiberg.se) to estimate global parameters for cardiac function. Scar size and location were derived from LGE images via semi-automatic segmentation using Segment. Segmented scar regions were exported following the American Heart Association (AHA) 17-segment model. Segments with >75% scar area were classified as scar segments for downstream analysis. Segments without scar were classified as the remote zone, whereas the remaining segments were classified as the border zone. Short-axis cine images were also used to estimate fractional shortening of the myocardium in the radial direction.

Tagged images were analyzed using the Strain from Unwrapped Phase (*SUP*) calculation method as previously described.[27] The *SUP* has the ability to reconstruct 3D ventricular strain maps from tagged MR images throughout the cardiac cycle. The analysis workflow included three steps: semi-automatic segmentation of the myocardial walls, phase corrections of the unwrapped phase, and generation of displacement maps to calculate myocardial strain (Figure 1B).

Based on finite deformation theory, the myocardial strain tensor (E) measures changes in myocardial shape during the cardiac cycle and is not affected by rigid-body motion. Shape changes along the long-axis, radial-axis, and circumference were used to calculate longitudinal, radial, or circumferential strain. We focused primarily on global and local circumferential strains for our analysis due to their reported ability for the detection of contraction impairment.[28] Negative peak circumferential strain (E_{cc}) was utilized to reflect myocardial contractility. Global E_{cc} was calculated by averaging circumferential strains across the heart. To compare regional differences, *Ecc* strain maps were converted to the AHA 17-segment model (without the 17th segment representing the apex) by averaging the voxel-based strains for each segment. These segments were grouped together as remote, scar, or border zone based on the LGE-derived tissue classification (Figure 1C). Additionally, time-to-peak strain was utilized to estimate myocardial asynchrony among different myocardial regions. Ten randomly selected rats were analyzed to estimate intra- and inter-observer variability for *Ecc* strain.

Ultrasound Imaging and Analysis

Speckle tracking-based ultrasound strain imaging was also performed on these experimental animals on D-1 and D28. Two-dimensional (2D) B-mode ultrasound images in short-axis view were acquired using a high frequency (21 MHz) linear transducer (MS250) connected to a small animal ultrasound system (Vevo 2100; VisualSonics, Toronto, Canada). Rats were sedated with 1–2% (v/v) isoflurane in oxygen and chests hairs were removed. 2D B-mode images were recorded in a short-axis view.

Cardiac ultrasound image series were analyzed using the VevoStrain software. After manual initialization, myocardial boundaries were automatically tracked throughout the cardiac cycle. Cardiac strains were calculated using speckle tracking. These strains were represented using an AHA 17-segment model, which only included mid-ventricular segments. Based on LGE MRI, these segments were classified as scar regions, remote, or border zones for comparisons. Intra- and inter-observer variability was also validated for ten randomly selected rats.

Histology

Serial sections from paraformaldehyde (PFA) fixed and optimal cutting temperature (OCT) embedded hearts were stained for human cardiac troponin T (Abcam, ab45932) and alpha actinin (Sigma, A7811) following previously published procedures.[5] Masson's trichrome staining was also performed using a standard protocol.[5] The scar sizes of 4 EHM versus 4 control hearts were measured by comparing the scar area with LV area in mid-ventricular short axis slices.

Statistical Analysis

All data sets were complete with no missing data points. Results are presented as mean ± SEM. To compare global and regional parameters for cardiac function, a mixed ANOVA was used to assess the time by treatment interaction effect on cardiac function by considering the within-subject correlation among measurements. For the comparisons of their changes, the difference between D-1 and D28 was calculated for each animal, followed by a Student's *t*-test to compare control and EHM treatment groups. The statistical analysis was performed using SPSS Statistics software (IBM, Armonk, NY). A value of $p < 0.05$ was considered significant.

RESULTS

Global measures of systolic function failed to detect significant differences between control and treatment groups

We have previously shown that EHM transplantation leads to long-term survival and engraftment of CMs (Figure 2A) as well as attenuated disease progression.[5] Here we performed strain imaging on a subset (EHM n=12, control n=10, healthy n=6) of these animals to test the capability of strain imaging for evaluating a localized regenerative therapy. Global cardiac parameters, including contractile function and scar size measurements, were quantified from cine MR images at D-1 and D28 (Supplemental Table 1). At D-1, there were no significant differences in end-diastolic volume (EDV; EHM 493.1±11.9 vs. control 449.6±17.9, p=0.07), end-systolic volume (ESV; EHM 218.0±19.0 vs. control 209.4±20.1, p=0.22), or EF (EHM 53.1±2.6% vs. control 54.2±2.8%, p=0.64) between EHM and control groups prior to EHM transplantation or sham surgery (Figure 2A).

EF is the most frequently used parameter to evaluate global contractile function of hearts. In this study, the EF changes from D-1 to D28 showed a similar decline for both EHM and control groups, thus failing to show a significant difference (EHM −6.2±1.9% vs. control −9.6±1.3%, P=0.17; Figure 3B). Scar size is another frequently used parameter to assess regenerative therapies. Although scar sizes increased slightly in the control group without changes being found for the EHM group from D-1 to D28, these changes were not statistically significant (EHM 0.01±1.0% vs. control 0.9±0.4%, P=0.07; Figure 3C, D). These findings were corroborated by Masson's trichrome staining, which also failed to detect differences in scar size at D28 (EHM 22.2 ±2.0% vs. control 22.5±3.5%, P=0.48; Figure 2D, E).

Cardiac MRI-based strain analysis

To assess the performance of strain imaging for evaluating localized regenerative therapies, we next compared both global and regional strain parameters measured from cardiac MRI of healthy, control, and EHM rats (Supplemental Table 2). We estimated the global circumferential strain by averaging voxel-based circumferential strains of the whole heart. Regional strain estimates were generated by grouping voxel-based strains for specific regions (scar and remote zone). The same grouping was used for fractional wall thickening and time-to-peak estimates.

Global circumferential strain was similar between treatment and control group

One month after EHM transplantation or sham surgery (control), global circumferential strains (*Ecc*) at D28 were similar for both groups (EHM −15.3±0.4% vs. control −13.5±1.0%, P=0.22). Both groups showed slight increases compared to baseline (D-1) (Figure 3E). Although this increase in circumferential strain Δ*Ecc* was larger in the control group compared to EHM (Control Δ*Ecc* 3.2±1.0% vs. EHM Δ*Ecc* 1.0±0.6%, Figure 3F), it did not reach statistical significance (P=0.08). Similar to estimates of global systolic function such as EF, global circumferential strain failed to detect a treatment effect due to EHM transplantation.

Regional circumferential strain showed therapeutic efficacy of EHM transplantation

Late gadolinium enhancement data were used to classify the 17 segments of the AHA model into scar, remote, and border zone groups. All regional estimates for cardiac performance were grouped together based on to this classification. Regional circumferential strain for the scar tissue *Ecc_scar* in the control group showed a significant increase (−13.5±1.6% D-1 to −9.1±1.1% D28, P=0.02), whereas the EHM group remained constant (−12.6±1.0% D-1 to −11.5±0.7% D28, P=0.39, Figure 4A). This increase in scar strain Δ*Ecc_scar* was significantly larger in the control group compared to EHM (Control Δ*Ecc_scar* 4.4±1.0% vs. EHM Δ*Ecc_scar* 1.0±0.6%, Figure 4B), indicating a preservation of contractile performance following EHM transplantation (P=0.04). However, cardiac strain in the EHM group did not revert to the level observed in the free wall of the healthy group (no MI −27.7±2.4%).

In contrast to regional circumferential strain, the change in regional wall thickening from D-1 to D28 (derived from cine data) in the scar region failed to detect significant differences between control and EHM groups (Control −4.2±3.0% vs. EHM −4.1±2.2%, P=0.98, Figure 4C, D).

Hearts with myocardial infarcts also showed lower circumferential strains in remote tissue compared to healthy controls (no MI). However, there were no significant differences for circumferential strain changes from D-1 to D28 in remote tissue between control and EHM groups (Control 3.8±1.0% vs. EHM 2.5±1.2%, P=0.42, Figure 4E, F).

Furthermore, to assess potential asynchrony between different segments of the heart, time-to-peak was analyzed in both scar region and remote zone. Although time-to-peak in the scar region showed a smaller increase in the EHM group compared to control (Control 13.4±0.3 vs. EHM 11.4±0.8, Figure 5A, B), this difference was not statistically significant (P=0.07). The time-to-peak in remote zone was similar for EHM and control groups (Control 10.9±0.5 vs. EHM 10.7±0.5, P=0.78, Figure 5C).

Ultrasound-based strain analysis failed to detect significant differences between control and treatment groups

Cardiac ultrasound is the most common imaging modality in cardiology. We therefore performed ultrasound-based strain analysis on the same animals that were used for MRI. We measured both global and regional circumferential strains (*Ecc*) from 2D ultrasound images by using the speckle tracking method (Figure 6). Different from MRI, ultrasound-based

analysis of localized strain was not able to detect significant differences between EHM and control group (Control −8.9±1.9 vs. EHM −10.2±1.6, P=0.47 for scar *Ecc*; Control −15.6±1.6 vs. EHM −15.2±1.9, P=0.73 for remote zone *Ecc*).

Reproducibility of strain analysis

Intra- and inter-observer variability was estimated for global and regional strain analysis from MRI and ultrasound data (Figure 7). Bland-Altman plots showed small systemic offsets for MRI and slightly larger ones for ultrasound. However, limits of agreement indicated that ultrasound had larger intra- and inter-observer variability than MRI.

DISCUSSION

The growing interest in localized cardiac regenerative therapies requires more accurate noninvasive methods to characterize functional benefits due to these interventions. We therefore set out to compare the capability of MRI and ultrasound-based techniques for regional assessment of cardiac function. Previous studies demonstrated the regenerative potential of EHM transplantation that led to long-term cell survival, high engraftment rates, and reduced disease progression.[3, 5] Although these studies were able to detect functional benefits based on the analysis of global systolic function, this required substantial group sizes (n >14). With the smaller group sizes used for the current study, EF failed to detect significant differences between EHM and control groups. This lack of successful detection likely arises from primarily localized benefits following EHM transplantation, which are difficult to detect on an organ level. Techniques that can measure contractile performance locally should hence offer higher detection abilities compared to global measurement techniques.

Strain imaging is expected to supply additional information for localized regenerative therapies, because it can directly and locally assess contractile deformations of the treated myocardium. Although some studies have utilized strain imaging from both tagged MRI and cardiac ultrasound to assess therapeutic efficacy,[29–31] its detection limits and limits of agreement for these localized regenerative therapies have not been evaluated. To fill this gap, we validated strain analysis by using 3D tagged MRI and 2D ultrasound imaging data from infarcted rat hearts before and after EHM transplantations or sham surgery (control).

As expected, global measures of systolic function failed to detect significant differences between control and EHM groups due to smaller group sizes used in the current study. By contrast, regional analysis detected the preservation of circumferential strain in the scar region following EHM transplantation. This illustrates the higher detection ability of localized strain analysis from tagged MRI data. Although EHM transplantation was sufficient to prevent the deterioration of circumferential strain in the scar region, it did not improve contractile performance. Fractional wall shortening is an estimate for 1D radial strain that can be derived from cine MRI or B-mode ultrasound data. Similar to global measures of cardiac function, it was unable to detect significant differences between control and treatment groups. This might be due a higher wall thickness in the scar region following ischemia reperfusion compared to permanent LAD occlusion used in a previous study.[3] Diseases or therapeutic interventions that affect the timing of myocardial contractions

differently across the heart can lead to cardiac dyssynchrony. Nonetheless, time-to-peak estimates for different regions of the hearts were not significantly different between control and EHM groups. One potential explanation for this may be that the human cells used to make EHMs were unable to contract at the rate of the host myocardium in this xenograft model. However, human cardiomyocytes might still induce therapeutic effects via paracrine mechansims.[3] Additionally, we assessed the reproducibility of 3D strain from the unwrapped phase technique by estimating the intra-observer variability. Strain analysis was performed automatically following manual initialization and phase correction. This led to small systematic biases of both global and regional strain as well as narrow limits of agreement, which were in line with previously published data.[19, 27, 32]

Due to its popularity and high temporal resolution, we decided to include ultrasound-based strain analysis in our study as well. Circumferential strain was calculated from 2D high-frequency ultrasound images using speckle tracking. While general trends were similar compared to MRI-based strain estimates, we were unable to detect any significant differences between control and treatment groups. Although ultrasound-based strain imaging has been validated for cardiac therapies in mice,[33] ultrasound images acquired from rats had a lower signal-to-noise-ratio (SNR) due to the poor ultrasound window in rats. Its detection ability was also limited by the 2D image acquisition because EHMs grafts covered less than half of the anterior free wall. Due to the small group sizes of the current study, these problems led to large variations within the analyzed groups. Larger group sizes could help to overcome this problem. In addition, we cannot definitely conclude that the localized strain measured from ultrasound was significantly different from that of tagged MRI since we only demonstrated that they fell on different sides of the critical test statistics.

In summary, this study demonstrates the feasibility of localized strain assessment for regenerative therapies. MRI-based strain was able to detect preservation of localized contractile function in rat hearts following EHM transplantation, a feat that could not be accomplished by global measures of systolic function. In contrast to MRI, ultrasound-based strain imaging failed to detect significant differences between control and treatment groups. This was primarily due to the limited ultrasound window in rats. Therefore, MRI-based strain may help illustrate the therapeutic mechanism of such therapies while simultaneously reducing group size requirements compared to global functional assessment.

Supplementary Material

Refer to Web version on PubMed Central for supplementary material.

Acknowledgments

We would like to thank Laura Pisani from Stanford Small Animal Imaging Facility for her help with MRI acquisition; Dr. Ming Li from Auburn University, Auburn, Alabama, for his technical assistance; Dr. Xin Ma from the Department of Statistics at Stanford University for statistical assistance, and Mouer Wang and Qi Shen for animal surgery and imaging.

Funding Sources

W.H. Zimmermann is supported by DZHK (German Center for Cardiovascular Research), German Federal Ministry for Science and Education (BMBF/CIRM FKZ 13GW0007A), German Research Foundation (DFG SFB 1002 C04

and 937 A18), European Union FP7 CARE-MI, Leducq Foundation, California Institute of Regenerative Medicine (CIRM) TR3-05556, and National Institutes of Health (NIH) U01 HL099997. J.C. Wu is supported by U01 HL099776, Leducq Foundation, CIRM RT3-07798, CIRM TR3-05556, and CIRM DR2A-05394.

References

1. Ye L, Zimmermann WH, Garry DJ, Zhang JY. Patching the heart: cardiac repair from within and outside. Circ Res. 2013; 113:922–932. [PubMed: 24030022]
2. Hirt MN, Hansen A, Eschenhagen T. Cardiac tissue engineering state of the Art. Circ Res. 2014; 114:354–367. [PubMed: 24436431]
3. Zimmermann WH, Melnychenko I, Wasmeier G, Didie M, Naito H, Nixdorff U, Hess A, Budinsky L, Brune K, Michaelis B, Dhein S, Schwoerer A, Ehmke H, Eschenhagen T. Engineered heart tissue grafts improve systolic and diastolic function in infarcted rat hearts. Nature Medicine. 2006; 12:452–458.
4. Ye L, Chang YH, Xiong Q, Zhang P, Zhang L, Somasundaram P, Lepley M, Swingen C, Su L, Wendel JS, Guo J, Jang A, Rosenbush D, Greder L, Dutton JR, Zhang J, Kamp TJ, Kaufman DS, Ge Y, Zhang J. Cardiac repair in a porcine model of acute myocardial infarction with human induced pluripotent stem cell-derived cardiovascular cells. Cell Stem Cell. 2014; 15:750–61. [PubMed: 25479750]
5. Riegler J, Tiburcy M, Ebert A, Tzatzalos E, Raaz U, Abilez OJ, Shen Q, Kooreman NG, Neofytou E, Chen V, Wang M, Meyer T, Tsao PS, Connolly AJ, Couture LA, Gold JD, Zimmermann WH, Wu JC. Human engineered heart muscles engraft and survive long-term in a rodent myocardial infarction model. Circ Res. 2015; 117:720–30. [PubMed: 26291556]
6. Naumova AV, Modo M, Moore A, Murry CE, Frank JA. Clinical imaging in regenerative medicine. Nature Biotechnology. 2014; 32:804–18.
7. Nguyen PK, Riegler J, Wu JC. Stem cell imaging: from bench to bedside. Cell Stem Cell. 2014; 14:431–44. [PubMed: 24702995]
8. Wendel JS, Ye L, Zhang P, Tranquillo RT, Zhang JJ. Functional consequences of a tissue-engineered myocardial patch for cardiac repair in a rat infarct model. Tissue Eng Part A. 2014; 20:1325–35. [PubMed: 24295499]
9. Chong JJ, Yang X, Don CW, Minami E, Liu YW, Weyers JJ, Mahoney WM, Van Biber B, Cook SM, Palpant NJ, Gantz JA, Fugate JA, Muskheli V, Gough GM, Vogel KW, Astley CA, Hotchkiss CE, Baldessari A, Pabon L, Reinecke H, Gill EA, Nelson V, Kiem HP, Laflamme MA, Murry CE. Human embryonic-stem-cell-derived cardiomyocytes regenerate non-human primate hearts. Nature. 2014; 510:273–7. [PubMed: 24776797]
10. Laflamme MA, Chen KY, Naumova AV, Muskheli V, Fugate JA, Dupras SK, Reinecke H, Xu C, Hassanipour M, Police S, O'Sullivan C, Collins L, Chen Y, Minami E, Gill EA, Ueno S, Yuan C, Gold J, Murry CE. Cardiomyocytes derived from human embryonic stem cells in pro-survival factors enhance function of infarcted rat hearts. Nat Biotechnol. 2007; 25:1015–24. [PubMed: 17721512]
11. Surder D, Manka R, Lo Cicero V, Moccetti T, Rufibach K, Soncin S, Turchetto L, Radrizzani M, Astori G, Schwitter J, Erne P, Zuber M, Auf der Maur C, Jamshidi P, Gaemperli O, Windecker S, Moschovitis A, Wahl A, Buhler I, Wyss C, Kozerke S, Landmesser U, Luscher TF, Corti R. Intracoronary injection of bone marrow-derived mononuclear cells early or late after acute myocardial infarction: effects on global left ventricular function. Circulation. 2013; 127:1968–79. [PubMed: 23596006]
12. La Gerche A, Claessen G, Van de Bruaene A, Pattyn N, Van Cleemput J, Gewillig M, Bogaert J, Dymarkowski S, Claus P, Heidbuchel H. Cardiac MRI: a new gold standard for ventricular volume quantification during high-intensity exercise. Circ Cardiovascular imaging. 2013; 6:329–38. [PubMed: 23258478]
13. Friedrich MG, Marcotte F. Cardiac magnetic resonance assessment of myocarditis. Circ Cardiovascular imaging. 2013; 6:833–9. [PubMed: 24046380]
14. Ibrahim el SH. Myocardial tagging by cardiovascular magnetic resonance: evolution of techniques--pulse sequences, analysis algorithms, and applications. J Cardiovasc Magn Reson. 2011; 13:36. [PubMed: 21798021]

15. Kraigher-Krainer E, Shah AM, Gupta DK, Santos A, Claggett B, Pieske B, Zile MR, Voors AA, Lefkowitz MP, Packer M, McMurray JJ, Solomon SD. Investigators P. Impaired systolic function by strain imaging in heart failure with preserved ejection fraction. J Am Coll Cardiol. 2014; 63:447–56. [PubMed: 24184245]
16. van Slochteren FJ, Teske AJ, van der Spoel TI, Koudstaal S, Doevendans PA, Sluijter JP, Cramer MJ, Chamuleau SA. Advanced measurement techniques of regional myocardial function to assess the effects of cardiac regenerative therapy in different models of ischaemic cardiomyopathy. Eur Heart J Cardiovasc Imaging. 2012; 13:808–18. [PubMed: 22707453]
17. Gorcsan J 3rd, Tanaka H. Echocardiographic assessment of myocardial strain. J Am Coll Cardiol. 2011; 58:1401–13. [PubMed: 21939821]
18. Ashikaga H, Leclercq C, Wang J, Kass DA, McVeigh ER. Hemodynamic improvement in cardiac resynchronization does not require improvement in left ventricular rotation mechanics: three-dimensional tagged MRI analysis. Circ Cardiovascular imaging. 2010; 3:456–63. [PubMed: 20478988]
19. Chen SS, Keegan J, Dowsey AW, Ismail T, Wage R, Li W, Yang GZ, Firmin DN, Kilner PJ. Cardiovascular magnetic resonance tagging of the right ventricular free wall for the assessment of long axis myocardial function in congenital heart disease. J Cardiovasc Magn Reson. 2011; 13:80. [PubMed: 22168638]
20. Kim D, Gilson WD, Kramer CM, Epstein FH. Myocardial tissue tracking with two-dimensional cine displacement-encoded MR imaging: development and initial evaluation. Radiology. 2004; 230:862–71. [PubMed: 14739307]
21. Zhong X, Gibberman LB, Spottiswoode BS, Gilliam AD, Meyer CH, French BA, Epstein FH. Comprehensive cardiovascular magnetic resonance of myocardial mechanics in mice using three-dimensional cine DENSE. J Cardiovasc Magn Reson. 2011; 13:83. [PubMed: 22208954]
22. Cikes M, Sutherland GR, Anderson LJ, Bijnens BH. The role of echocardiographic deformation imaging in hypertrophic myopathies. Nat Rev Cardiol. 2010; 7:384–96. [PubMed: 20458340]
23. Hoit BD. Strain and strain rate echocardiography and coronary artery disease. Circ Cardiovascular imaging. 2011; 4:179–90. [PubMed: 21406664]
24. Boyd AC, Schiller NB, Thomas L. Principles of transthoracic echocardiographic evaluation. Nat Rev Cardiol. 2015; 12:426–40. [PubMed: 25917151]
25. Chen VC, Couture SM, Ye J, Lin Z, Hua G, Huang HI, Wu J, Hsu D, Carpenter MK, Couture LA. Scalable GMP compliant suspension culture system for human ES cells. Stem Cell Research. 2012; 8:388–402. [PubMed: 22459095]
26. Tiburcy M, Meyer T, Soong PL, Zimmermann WH. Collagen-based engineered heart muscle. Methods Mol Biol. 2014; 1181:167–76. [PubMed: 25070336]
27. Venkatesh BA, Gupta H, Lloyd SG, Dell 'Italia L, Denney TS Jr. 3D left ventricular strain from unwrapped harmonic phase measurements. J Magn Reson Imaging. 2010; 31:854–62. [PubMed: 20373429]
28. Helm RH, Leclercq C, Faris OP, Ozturk C, McVeigh E, Lardo AC, Kass DA. Cardiac dyssynchrony analysis using circumferential versus longitudinal strain - Implications for assessing cardiac resynchronization. Circulation. 2005; 111:2760–2767. [PubMed: 15911694]
29. Vallee JP, Hauwel M, Lepetit-Coiffe M, Bei W, Montet-Abou K, Meda P, Gardier S, Zammaretti P, Kraehenbuehl TP, Herrmann F, Hubbell JA, Jaconi ME. Embryonic stem cell-based cardiopatches improve cardiac function in infarcted rats. Stem Cells Transl Med. 2012; 1:248–60. [PubMed: 23197784]
30. Macarthur JW Jr, Cohen JE, McGarvey JR, Shudo Y, Patel JB, Trubelja A, Fairman AS, Edwards BB, Hung G, Hiesinger W, Goldstone AB, Atluri P, Wilensky RL, Pilla JJ, Gorman JH 3rd, Gorman RC, Woo YJ. Preclinical evaluation of the engineered stem cell chemokine stromal cell-derived factor 1alpha analog in a translational ovine myocardial infarction model. Circ Res. 2014; 114:650–9. [PubMed: 24366171]
31. Yamada S, Nelson TJ, Kane GC, Martinez-Fernandez A, Crespo-Diaz RJ, Ikeda Y, Perez-Terzic C, Terzic A. Induced pluripotent stem cell intervention rescues ventricular wall motion disparity, achieving biological cardiac resynchronization post-infarction. J Physiol. 2013; 591:4335–49. [PubMed: 23568891]

32. Venkatesh BA, Schiros CG, Gupta H, Lloyd SG, Dell'Italia L, Denney TS Jr. Three-dimensional plus time biventricular strain from tagged MR images by phase-unwrapped harmonic phase. J Magn Reson Imaging. 2011; 34:799–810. [PubMed: 21769965]

33. Bauer M, Cheng S, Jain M, Ngoy S, Theodoropoulos C, Trujillo A, Lin FC, Liao R. Echocardiographic speckle-tracking based strain imaging for rapid cardiovascular phenotyping in mice. Circ Res. 2011; 108:908–16. [PubMed: 21372284]

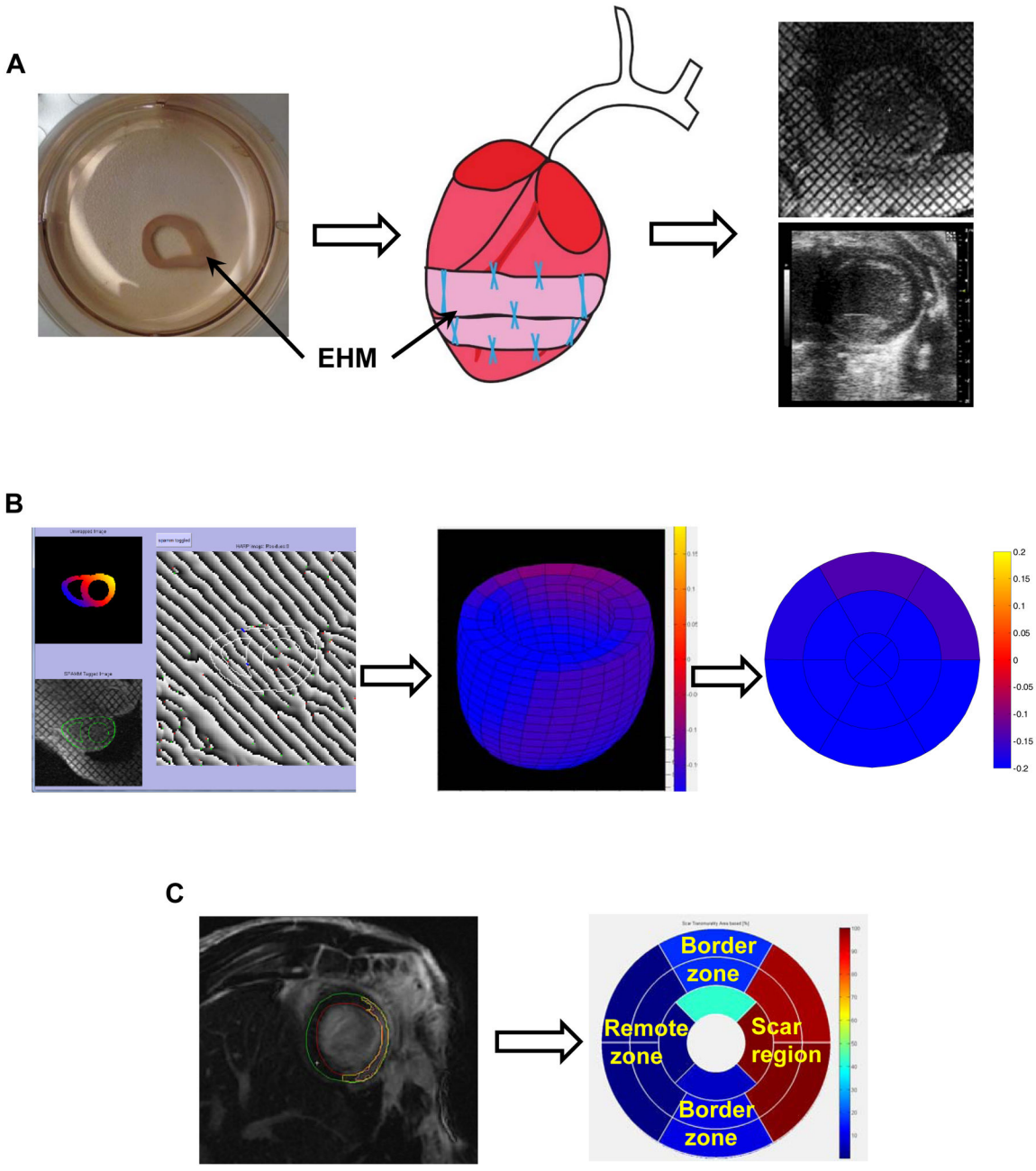

Figure 1. Flowchart illustrating strain analysis in both scar and remote zone following EHM transplantation

(A) Schematic illustrating an EHM loop after functional maturation, sutured over the scar region with 8–12 stiches, and monitored noninvasively with different strain imaging techniques. **(B)** Strain analysis from tagged MRI using a Strain from Unwrapped Phase (SUP) method to calculate the localized strain throughout the heart and its conversion into the 17-segment AHA model. **(C)** Scar volumes (yellow line) were estimated from late gadolinium-enhanced images and converted into the AHA 17-segment model to define both scar (red) and remote zone (dark blue) based on fraction of scar tissue present in different segments. EHM: engineered heart muscle.

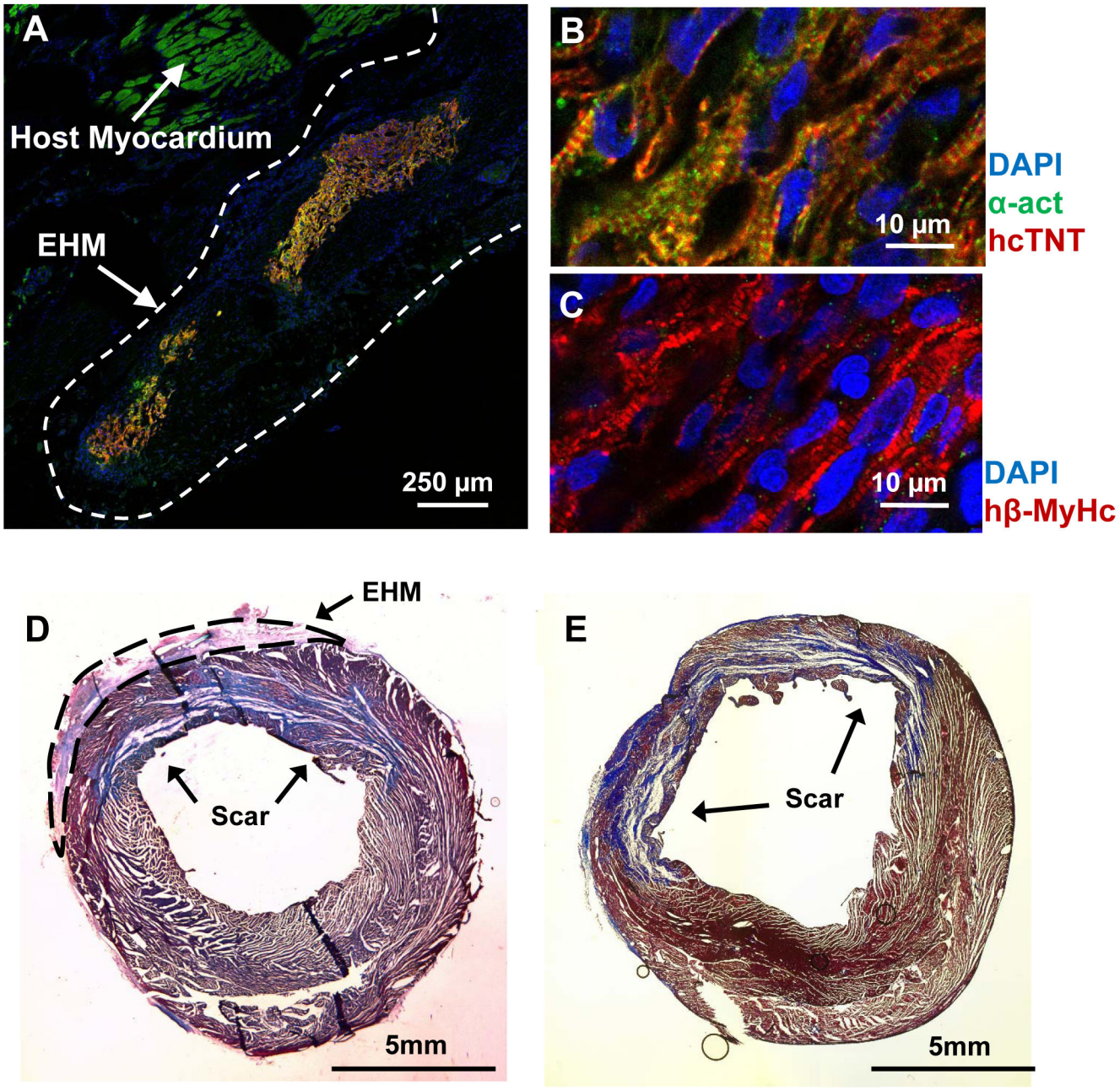

Figure 2. Immunofluorescence showed viable human cardiomyocytes 4 weeks after transplantation of engineered heart muscle

(A) Transplanted engineered heart muscle (EHM) led to the engraftment of human cardiomyocytes on the host heart. Partially aligned sarcomeres could be detected in viable human cardiomyocytes when staining for (**B**) alpha actinin (α-act), human cardiac troponin T (hcTnT), and (**C**) human beta myosin heavy chain (hβ-MyHc). Despite substantial engraftment and survival of human cardiomyocytes, scar sizes between **(D)** EHM (n=4) and **(E)** control groups (n=4) were similar (p=0.48) as assessed by Masson' trichrome staining (blue color).

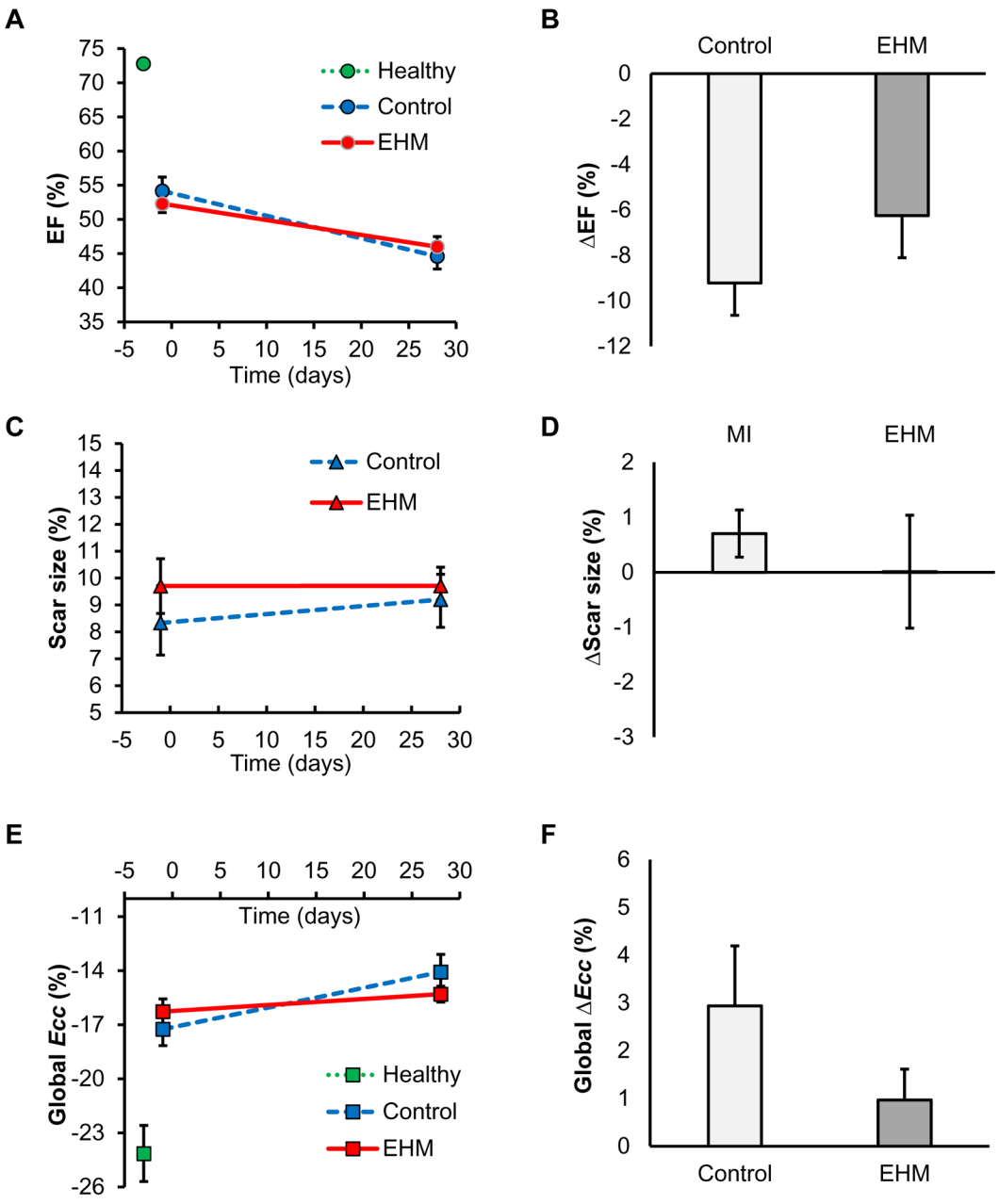

Figure 3. Global assessment of systolic function failed to show differences between EHM and control groups

No significant differences between EHM and control groups were detected by analyzing parameters of global function as well as their changes over time: **(A)** ejection fraction (EF), **(B)** change in EF, **(C)** scar size (percentile of LV mass), **(D)** change in scar size, **(E)** global strain, and **(F)** change in global strain. EHM: engineered heart muscle treated group. E_{cc}: negative peak of circumferential strain.

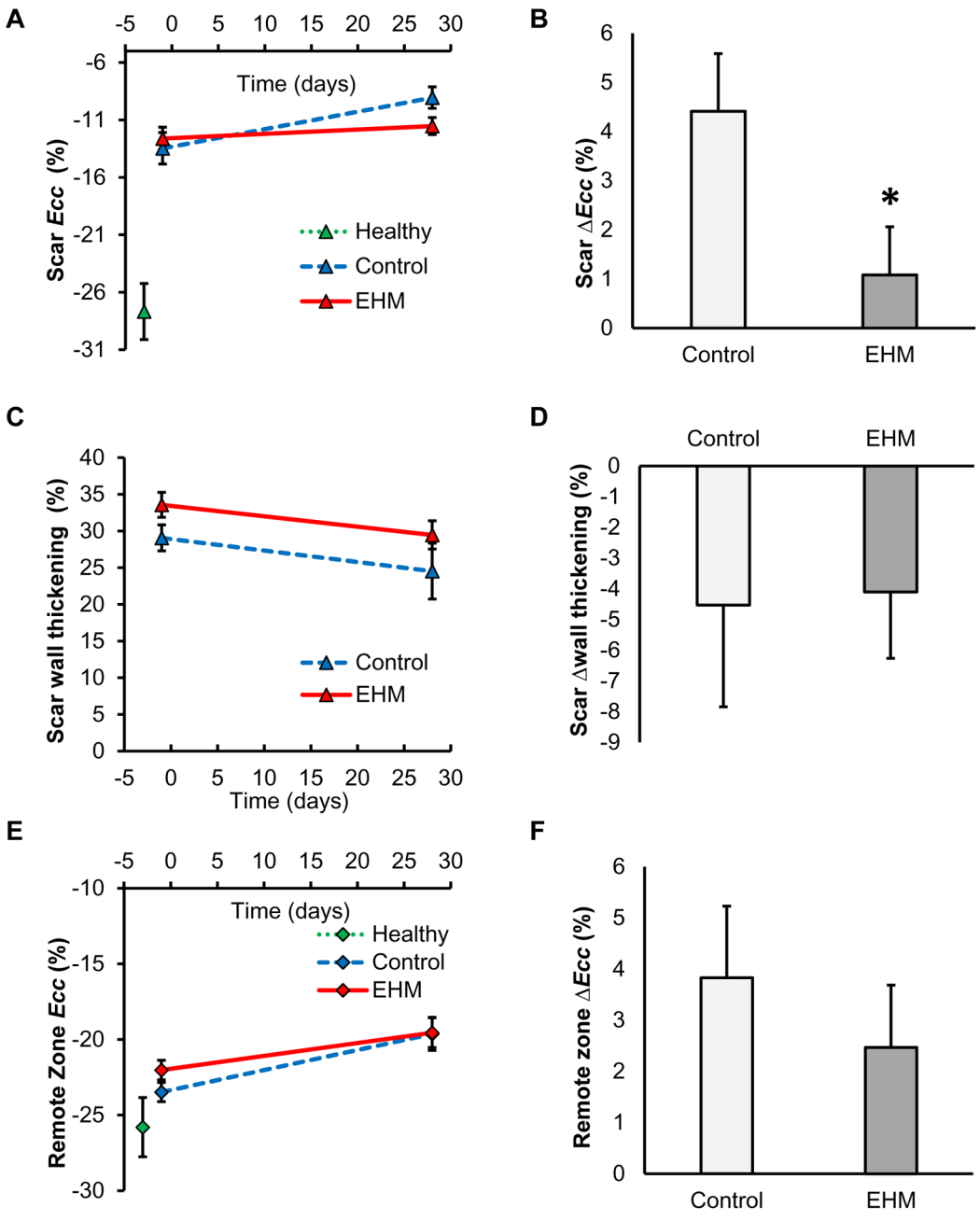

Figure 4. Regional circumferential strain showed preservation of contractile performance in the EHM group compared to control

Regional function assessed from cardiac MRI included **(A)** regional strain in the scar region, **(C)** wall thickening in the scar region, and (**E**) regional strain in the remote zone. Significant differences between both EHM and control groups were detected for **(B)** changes in regional strain in the scar region, but not for changes in other parameters or regions such as **(D)** change in wall thickening or **(F)** change in regional strain of the remote zone. E_{cc}: negative peak of circumferential strain. * P<0.05.

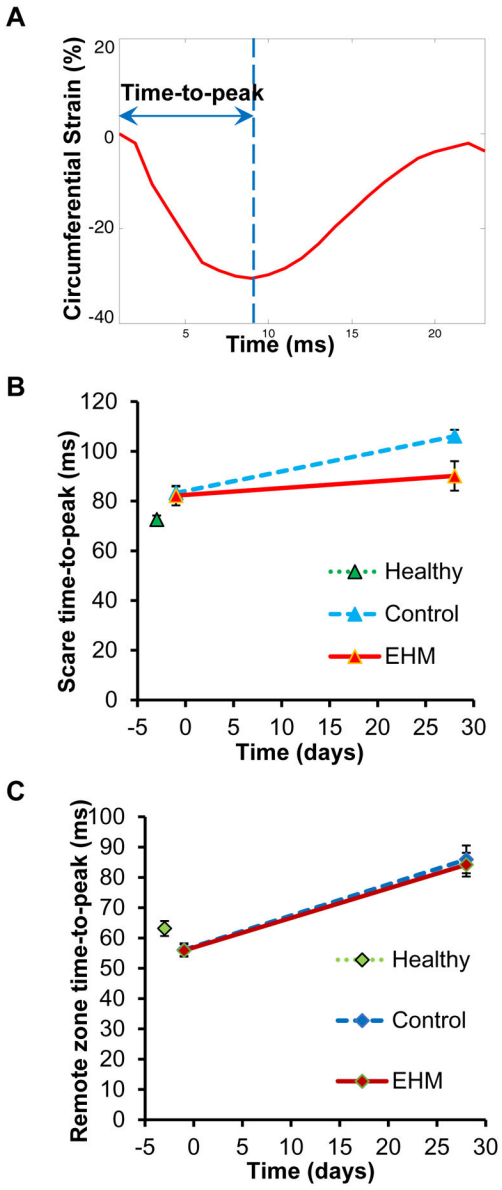

Figure 5. Analysis of cardiac synchrony failed to detect differences between control and EHM groups

(A) Time-to-peak was defined as the time delay between the starting frame and negative peak of circumferential strain. **(B)** A non-significant increase in time-to-peak was found for the control group compared to EHM. **(C)** Time-to-peak of the remote zone was similar for EHM and control groups. EHM: engineered heart muscle treated group.

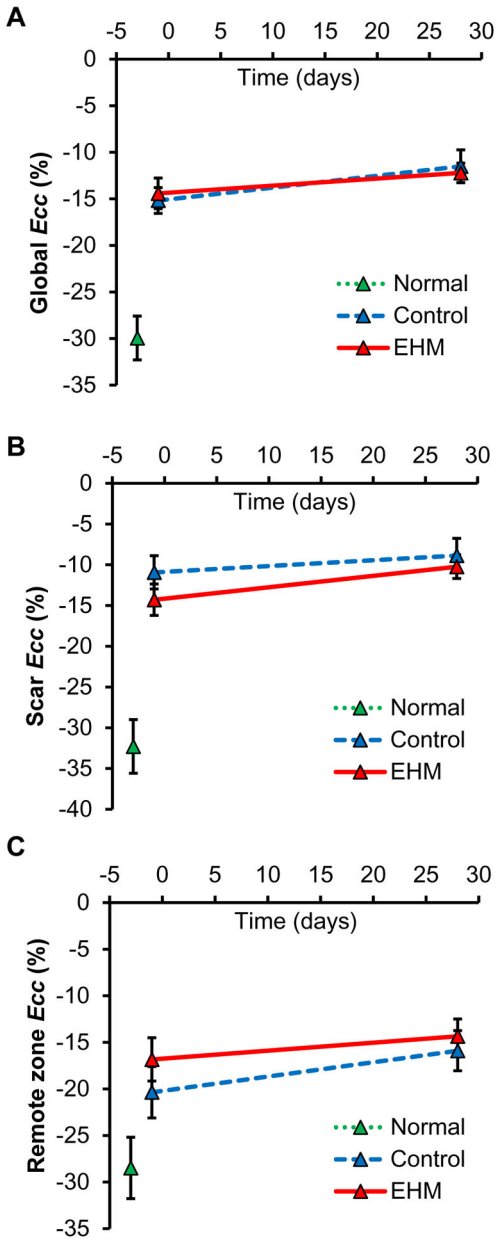

Figure 6. Ultrasound-based strain analysis failed to detect significant differences between treatment and control groups

No significant differences between EHM and control groups were detected by ultrasound imaging based strain analysis due to its greater variability. The analysis included the following parameters: **(A)** global strain, **(B)** regional strain in the scar region, and **(C)** regional strain in the remote zone. E_{cc}: negative peak of circumferential strain.

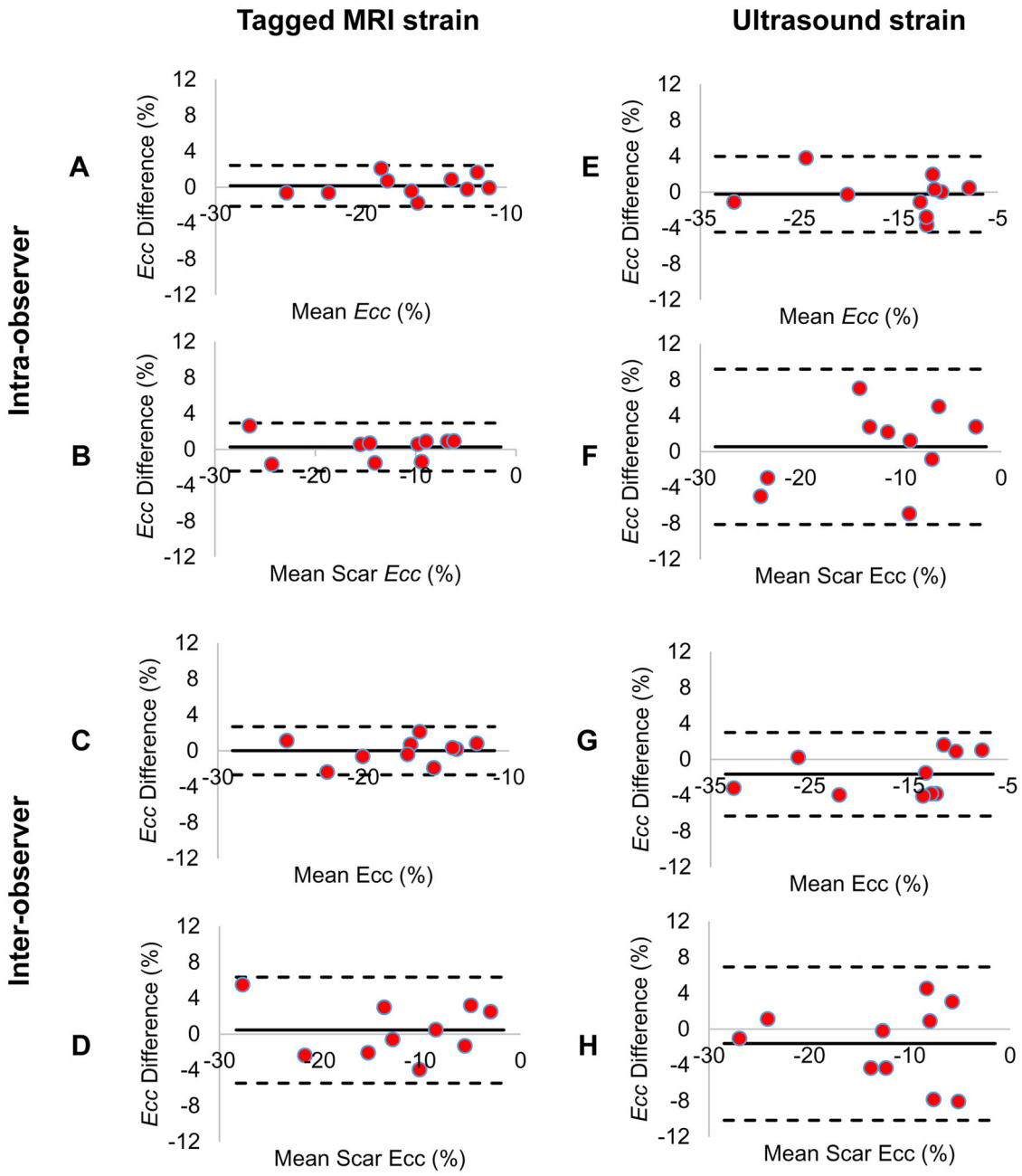

Figure 7. Reproducibility of MRI and ultrasound based strain analysis

The reproducibility of global and regional strain analysis for cardiac MRI and ultrasound were assessed by both intra- and inter-observer comparisons. Bland-Altman plots showed that systematic biases for global strains **(A, C)** and regional strains **(B, D)** from cardiac MRI were smaller than global strains **(E, G)** and regional strain biases **(F, H)** from ultrasound. Moreover, the 95% limits of agreement for MRI based strain were narrower than those for ultrasound. These results demonstrate a higher reproducibility of strain analysis from MRI data compared to ultrasound. E_{cc}: negative peak of circumferential strain.